International Immunopharmacology 142 (2024) 113154

Contents lists available at ScienceDirect

International Immunopharmacology

journal homepage: www.elsevier.com/locate/intimp

Efficacy of DHA-enriched phosphatidylserine and its underlying mechanism in alleviating polystyrene nanoplastics-induced hepatotoxicity in mice

Yuanlei Zhang [a], Qiaoling Zhao [b], Rui Zhao [a], Yun Lu [c,*], Su Jiang [d], Yunping Tang [a,*]

[a] School of Food and Pharmacy, Zhejiang Ocean University, Zhoushan, 316022, China
[b] Zhoushan Institute for Food and Drug Control, Zhoushan, 316000, China
[c] Medical Department, The Second Affiliated Hospital of Jiaxing University, Jiaxing, 314000, China
[d] ECA Healthcare Inc, Shanghai, 201101, China

ARTICLE INFO

Keywords:
Polystyrene nanoplastics
DHA-PS
Hepatotoxicity
Gut-liver axis
Multi-omics

ABSTRACT

Objective: Plastic pollution has become a global pollution problem that cannot be ignored. As the main destination of human oral intake, the toxic effects of plastic on the digestive system represented by the intestine and liver are the focus of current research. Marine-derived DHA-PS has a variety of biological activities, mainly focusing on improving brain function and regulating lipid metabolism. However, whether it has an improvement effect on PS-NPs-induced hepato-intestinal injury and the underlying mechanism remain unclear.

Methods: A murine liver injury model was established by gavage of PS-NPs for six weeks. By integrating approaches from lipidomics, transcriptomics, and gut microbiota analysis, the molecular mechanism by which DHA-PS alleviates PS-NPs-induced murine hepatotoxicity was explored through the "gut-liver axis".

Results: Our findings reveal that prolonged exposure to PS-NPs results in significant murine liver damage and dysfunction, characterized by increased oxidative stress and inflammation, along with exacerbated hepatic lipid accumulation. Mechanistically, PS-NPs disrupt the hepatic SIRT1-AMPK pathway by suppressing the expression of SIRT1, AMPKα, and PPARα, while enhancing the expression of SREBP-1c, ultimately leading to disordered hepatic lipid metabolism. The sphingolipid and glycerophospholipid metabolic pathways were particularly affected. Additionally, in agreement with transcriptomic analyses, PS-NPs activate the hepatic TLR4/NF-κB pathway. At the same time, exposure to PS-NPs decreases the expression of ZO-1, occludin, and claudin-1, diminishes the relative abundance of beneficial gut bacteria (*norank_f_Muribaculaceae*, *Akkermansia*, and *norank_f_norank_o_Clostridia_UCG-014*), and increases the prevalence of pathogenic gut bacteria (*Coriobacteriaceae_UCG-002* and *Desulfovibrio*), exacerbating liver injury through the gut-liver axis. However, administering DHA-PS (50 mg/kg) effectively alleviated these injuries.

Conclusion: This study was the first to employ multi-omics techniques to elucidate the potential mechanisms underlying hepatotoxicity induced by PS-NPs, thereby supporting the use of DHA-PS as a dietary supplement to mitigate the effects of nanoplastic pollutants.

1. Introduction

Plastics, now a widespread global polluter, can break down into smaller fragments such as microplastics (MPs, <5 mm) and nanoplastics (NPs, <100 nm) through processes like photooxidation, wave action, and chemical reactions [1,2]. These particles, including MPs and NPs, are ubiquitously dispersed in the environment and can be found in varying concentrations in the air, drinking water, various seafood, fast food takeout, and other foods packaged in plastic [3,4]. In daily life, humans can intake MPs/NPs not only through consumption but also via breathing and skin contact [5,6]. Recently, researchers have shown that MPs/NPs can cause various health issues, including gastrointestinal, neurologic, hepatic, renal, developmental, and reproductive toxicity [7,8]. Consequently, the adverse impacts of MPs/NPs on human health and the development of strategies to mitigate these effects have emerged as significant concerns.

The gastrointestinal tract serves as the primary exposure pathway for MPs and NPs, whose ingestion has been proven to harm intestinal epithelial cells, alter gut microbiota, and impair intestinal barrier functions [9,10]. At this point, MPs/NPs distributed within the

* Corresponding authors.
E-mail addresses: jxeyluyun@126.com (Y. Lu), tangyunping1985@zjou.edu.cn (Y. Tang).

https://doi.org/10.1016/j.intimp.2024.113154
Received 6 June 2024; Received in revised form 29 August 2024; Accepted 9 September 2024

gastrointestinal tract can enter the liver via the portal vein, ultimately leading to liver toxicity [11]. Recently, the focus on the "gut-liver axis" has revealed significant insights into the relationship between the intestinal mucosal barrier, gut microbiota, metabolites, and their collective role in developing liver injury [12–14]. The disturbance of the "gut-liver axis" is characterized by intestinal barrier dysfunction, bacterial translocation and inflammation, and the activation of the toll-like receptor (TLR) pathway, all of which are crucial in the onset of various liver diseases [15,16]. Therefore, understanding the dynamics of the "gut-liver axis" provides a novel perspective for devising strategies to repair hepatic and intestinal damage potentially caused by MPs/NPs.

With the rapid development of the marine food processing industry, a large amount of by-products (heads, skins, viscera, bones, roes) are discarded, causing not only economic losses but also serious environmental pollution [17,18]. However, these by-products are rich in polyunsaturated fatty acids, proteins, etc., which can be converted into high-value-added products through enzyme catalysis or fermentation [19,20]. Specifically, docosahexaenoic acid-enriched phosphatidylserine (DHA-PS) can be synthesized from marine roes-derived DHA-enriched phosphatidylcholine (DHA-PC) using recombinant phospholipase D (PLD) [21]. Researchers have shown that DHA-PS possesses various biological functions, including enhancing memory, protecting liver and kidney health, regulating lipid metabolism, and improving gut microbiota balance [21,22]. However, there is currently no report on whether DHA-PS has a mitigating effect on murine liver injury induced by NPs exposure. In this study, a murine liver injury model was established by gavage of polystyrene nanoplastics (PS-NPs) for six weeks. By integrating approaches from lipidomics, transcriptomics, and gut microbiota analysis, we explored the molecular mechanism by which DHA-PS alleviates PS-NPs-induced murine hepatotoxicity through the "gut-liver axis", offering novel insights into counteracting the toxic effects of PS-NPs.

2. Materials and methods

2.1. Materials and reagents

DHA-PS was prepared by our research group as previously described [23]. The content of PS in the final product was 60.51%, and DHA and EPA in the total fatty acids were 34.1% and 12.2%, respectively. PS-NPs (100 nm) were provided by Zhongke Leiming (Beijing, China). Reagent kits for alanine aminotransferase (ALT), aspartate aminotransferase (AST), total cholesterol (TC), triglyceride (TG), non-esterified fatty acid (NEFA), malondialdehyde (MDA), superoxide dismutase (SOD), catalase (CAT), glutathione peroxidase (GSH-Px) and total antioxidant capacity (T-AOC) were purchased from Jiancheng (Nanjing, China). The ELISA kits of interleukin (IL)-1β, IL-6, IL-10, and tumor necrosis factor-α (TNF-α) were purchased from Elabscience Biotechnology (Wuhan, China) or Solarbio (Beijing, China). Hematoxylin-eosin (H&E) staining kit and Oil Red O staining kit were purchased from Beyotime Biotechnology (Shanghai, China). The lipopolysaccharides (LPS) kit was provided by Xiamen Bioendo Technology (Xiamen, China) for the assessment of LPS levels. Primary antibodies against SIRT1, AMPKα, PPARα, SREBP-1c, Claudin-1, Occludin, and ZO-1 were supplied by Proteintech Group (Wuhan, China).

2.2. Animal treatments

Animal experiments were approved by the Animal Ethics Committee of Zhejiang Ocean University (NO. 2022021) and conducted in SPF-grade animal facilities. Before the experiment, the DHA-PS solution and PS-NPs were sonicated for 30 min. After one week of adaptation feeding, male C57BL/6J mice (n = 18, 6 weeks old, 15 – 17 g) were randomly divided into CON group, MOD group, and DHA-PS group (n = 6 per group). Mice in the CON group were orally gavaged with Milli-Q water, while those in the MOD and DHA-PS groups were administered 25 mg/kg PS-NPs in an equal volume [21]. Additionally, mice in the DHA-PS group were orally gavaged with 50 mg/kg DHA-PS 30 min after PS-NPs administration daily for 6 weeks (Fig. 1A). On the last day of dosing, all mice were fasted for 12 h but allowed free access to water, and feces were collected under sterile conditions for gut microbiota analysis. Blood was collected by eyeball extraction, and mice were euthanized by cervical dislocation. Liver and jejunum tissues were dissected, frozen, and stored at −80 ℃. The murine liver index was calculated as follows: liver index (%) = liver weight (g) / body weight (g) × 100%.

2.3. Determination of biochemical indicators

The levels of LPS, ALT, and AST in serum were determined using respective assay kits. The frozen liver tissues were homogenized in physiological saline at a ratio of 1:9 (m/v), and the supernatant obtained after centrifugation was used to measure the LPS, TC, TG, NEFA, IL-1β, IL-6, IL-10, TNF-α, MDA content, as well as the CAT, SOD, GSH-Px, and T-AOC activities in liver tissue homogenates.

2.4. Histopathological and immunohistochemical analysis

After fixation in 4% paraformaldehyde, the fresh liver, and jejunum tissues were embedded in paraffin and sectioned. H&E and Oil Red O staining procedures were performed as previously described [24]. Additionally, liver sections were incubated with primary antibodies (SIRT1, AMPKα, SREBP-1c, PPARα), and jejunum sections were incubated with other primary antibodies (Claudin-1, Occludin, and ZO-1), followed by color development with DAB staining solution. Staining intensity was observed under a CX31 optical microscope and analyzed using Image J 1.52i software.

2.5. Western blotting

The expression levels of relevant proteins in the NF-κB pathway in mouse liver were assessed, and the primary antibodies were as follows: TLR4, p65, p-P65, IκBα, and p-IκBα. The target protein bands after visualization were subjected to semi-quantitative analysis using Alpha View software.

2.6. Lipidomic analysis

The fresh liver tissue samples (50 mg) were added with 280 μL of extract liquid (methanol : water = 2:5) and 400 μL methyl tert-butyl ether (MTBE), then frozen and ground for 6 min. The samples were extracted by ultrasound at low temperature for 30 min and then centrifuged at high speed (13,000 g, 4 ℃) for 15 min. Then, 350 μL of supernatant was removed, dried under nitrogen gas, and redissolved by adding 100 μL of compound solution (isopropanol : acetonitrile = 1:1). After vortexing and mixing, the mixture was sonicated and centrifuged for 10 min, and the supernatant was removed for LC-MS/MS analysis. Metabolite information was obtained by matching with the database. The data were analyzed through the free online platform of Majorbio cloud platform (cloud.majorbio.com). The PCA and OPLS-DA were performed using the R package ropls (version 1.6.2). Permutation tests were conducted to evaluate the stability of the model. Lipid metabolites showing intergroup differences were selected based on the criteria of VIP > 1 and $P < 0.05$, and key metabolic pathways were screened using the KEGG database.

2.7. Transcriptomic analysis

Transcriptomic analysis was performed by Majorbio (Shanghai, China). The fresh liver tissue (50 mg) was ground in liquid nitrogen and then mixed with 1 mL of Trizol at room temperature for 5 min. The supernatant was centrifuged (4 ℃, 13,000 g, 5 min), and 200 μL of

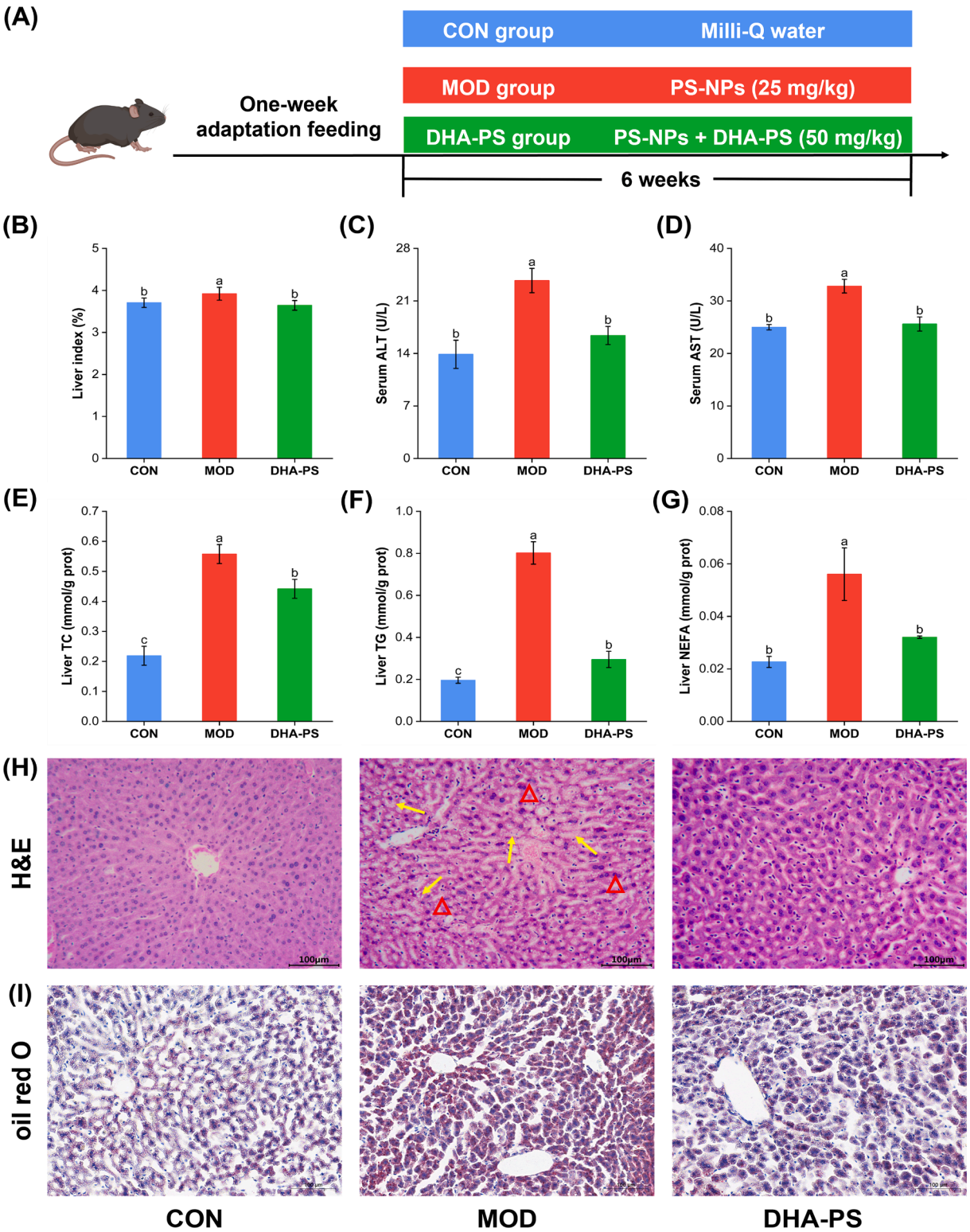

Fig. 1. Effect of DHA-PS on liver damage and lipid deposition induced by PS-NPs exposure in mice ($n = 6$). (A) Experimental design; (B) Liver index; (C) Serum ALT; (D) Serum AST; (E) Liver TC; (F) Liver TG; (G) Liver NEFA; (H) Liver H&E staining (200×; scale bar 100 μm). Disarrangement of hepatic cords (red triangles), vacuolar lesions (yellow arrows); (I) Liver Oil red O staining (200×; scale bar 100 μm). The English letters a, b, c represent the statistical results respectively, and different letters indicate significant differences between groups ($P < 0.05$). The same letter indicated no statistical difference between groups ($P > 0.05$). Unless otherwise stated, the same applies below.

precooled chloroform was added. The mixture was shaken and placed at room temperature for 5 min. 400 μL of the supernatant was centrifuged again, and an equal volume of precooled isopropanol was added and left for 10 min at room temperature. The supernatant was discarded by centrifugation and the RNA precipitate was washed by adding 1 mL of precooled 75% ethanol. Finally, the supernatant was removed by centrifugation, the RNA precipitate was allowed to dry at room temperature for 3–5 min, and dissolved by adding 20–50 μL of sterilized

0.1% DEPC water. The Illumina platform was used for library sequencing and bioinformatics analysis. Differential expression analysis was performed using DESeq2, with criteria set at $P < 0.05$ and $|\log2\ FC| \geq 1$ to identify intergroup differentially expressed genes (DEGs). Subsequent biological function and pathway enrichment analyses of DEGs were performed using the GO database and the KEGG database, respectively.

2.8. 16S rRNA sequencing

Mouse fecal sample DNA was extracted and amplified using primers 338F and 806R for PCR. Sequencing was performed using the Illumina MiSeq platform, and subsequent quality control and filtering were applied to the sequences. The α and β diversity analyses were conducted at the OTU level, and microbial community composition was analyzed at the phylum and genus levels. Kruskal-Wallis rank-sum test was employed to select significantly different microbial communities between groups. Differential species at various levels were identified using LEfSe analysis, and the effect size of differences in species abundance was evaluated using LDA values.

2.9. Statistical analysis

The experimental data were analyzed using one-way analysis of variance (ANOVA) and LSD post hoc test in SPSS 27.0 software. Results are presented as mean ± standard deviation ($\bar{x} \pm SD$), with $P < 0.05$ indicating significant differences between groups.

3. Results

3.1. DHA-PS alleviates liver injury and lipid deposition induced by PS-NPs

As illustrated in Fig. 1B, exposure to PS-NPs resulted in a notable elevation of the liver index compared to the CON (3.92 ± 0.15 *vs* 3.71 ± 0.11 mg/g, $P < 0.05$). After supplementing with DHA-PS, the liver index of mice notably decreased (3.64 ± 0.12 *vs* 3.92 ± 0.15 mg/g, $P < 0.05$). As important indicators for evaluating the degree of liver damage, the serum levels of ALT and AST significantly increased in the MOD (ALT: 23.72 ± 1.62 *vs* 13.89 ± 1.88 U/L, AST: 32.81 ± 1.30 *vs* 24.99 ± 0.51 U/L, $P < 0.05$, Fig. 1 C-D), and significantly decreased in the DHA-PS group (ALT: 16.39 ± 1.21 *vs* 23.72 ± 1.62 U/L, AST: 25.60 ± 1.34 *vs* 32.81 ± 1.30 U/L, $P < 0.05$), indicating that DHA-PS can improve the abnormal liver function induced by PS-NPs.

Meanwhile, in the MOD, the hepatic TC (0.56 ± 0.03 *vs* 0.22 ± 0.03 mmol/g prot, $P < 0.05$), TG (0.80 ± 0.05 *vs* 0.20 ± 0.01 mmol/g prot, $P < 0.05$), and NEFA (0.06 ± 0.01 *vs* 0.02 ± 0.00 mmol/g prot, $P < 0.05$) levels were notably enhanced compared to the CON (Fig. 1E–G). In the DHA-PS group, the above lipid levels were notably decreased (TC: 0.44 ± 0.03 *vs* 0.56 ± 0.03 mmol/g prot, TG: 0.29 ± 0.04 *vs* 0.80 ± 0.05 mmol/g prot, NEFA: 0.03 ± 0.00 *vs* 0.06 ± 0.01 mmol/g prot, $P < 0.05$). The H&E staining results (Fig. 1H) exhibited that in the CON, the liver structure was intact with clear radial arrangement of hepatic cords and no hepatocyte necrosis. PS-NPs caused severe damage to the liver structure, with the disordered arrangement of hepatic cords and the appearance of vacuolar degeneration. Nevertheless, treatment with DHA-PS notably ameliorated the pathological alterations in liver tissue, restoring the organization of hepatic cords and diminishing vacuolar degeneration. Additionally, the Oil Red O staining results (Fig. 1I) indicated that PS-NPs intake promoted lipid droplet accumulation in the liver, and DHA-PS treatment could significantly alleviate this phenomenon.

3.2. DHA-PS alleviates inflammation and oxidative stress induced by PS-NPs

When intestinal barrier function is impaired, LPS is released into the bloodstream and reaches the liver via the portal vein, triggering systemic or local inflammatory responses [25]. Compared to the CON, the LPS levels in the serum and liver, as well as hepatic IL-6, IL-1β, and TNF-α levels, were notably increased in the MOD, while the IL-10 level was notably decreased ($P < 0.05$, Table 1). However, the above indicators were notably reversed after DHA-PS treatment. Meanwhile, PS-NPs notably inhibited the activity of hepatic CAT, SOD, GSH-Px, and T-AOC, reducing them by 25.07%, 26.55%, 54.96%, 33.33%, respectively, and notably increased the MDA content ($P < 0.05$, Table 1). Supplementing with DHA-PS enhanced the activity of antioxidant enzymes and down-regulated the MDA levels. The changes in the above indicators suggest that DHA-PS can regulate cytokine secretion and enhance antioxidant capacity, thereby alleviating liver inflammation and oxidative stress.

3.3. Hepatic lipidomics analysis

Lipidomics was employed to investigate the potential mechanisms of DHA-PS in alleviating liver injury, and the metabolic characteristics of each group are shown in Fig. 2. The PCA score plot showed a certain degree of separation among the CON, MOD, and DHA-PS groups in both positive and negative ion modes, suggesting that exposure to PS-NPs and supplementation with DHA-PS affected the liver lipid profile in mice (Fig. 2A, D). Further validation of inter-group lipid metabolites was conducted using OPLS-DA analysis, and the stability of the model was assessed through permutation tests ($n = 200$). As shown in Fig. 2B,C and E,F, significant dispersion was observed in the MOD *vs* CON and DHA-PS *vs* MOD comparison groups in both positive and negative ion modes. The R^2Y values of the model parameters for each group were close to 1, and $Q^2 > 0.5$ (Supplementary Fig. S1), indicating good predictive capability of the model without overfitting. Additionally, differential lipid metabolites in the liver were screened based on selection criteria (VIP > 1 and $P < 0.05$), and the changes in different metabolites were visually displayed through volcano plots (Fig. 2G, H). A total of 454 differentially metabolites were identified in the MOD *vs* CON comparison group, including 276 up-regulated metabolites and 178 down-regulated metabolites; while 174 differentially metabolites were detected in the DHA-PS *vs* MOD comparison group, including 80 upregulated metabolites and 94 downregulated metabolites. Moreover, Venn diagram was used to show the difference and overlap of lipid metabolites in different alignment groups (Fig. 2I).

The clustering heatmap (Supplementary Fig. S2 and Table S1)

Table 1
Effect of DHA-PS on LPS levels, liver inflammation, and oxidative stress induced by PS-NPs in mice.

Index	CON	MOD	DHA-PS
Serum LPS (EU/mL)	0.73 ± 0.04 ^{b}	1.14 ± 0.01 ^{a}	0.84 ± 0.10 ^{b}
Liver LPS (EU/mL)	1.18 ± 0.02 ^{c}	2.89 ± 0.02 ^{a}	1.67 ± 0.14 ^{b}
Liver IL-10 (ng/mL)	8.62 ± 0.04 ^{a}	6.19 ± 0.34 ^{c}	7.25 ± 0.04 ^{b}
Liver IL-6 (ng/mL)	6.12 ± 0.05 ^{c}	9.29 ± 0.22 ^{a}	7.65 ± 0.43 ^{b}
Liver IL-1β (pg/mL)	767.09 ± 27.26 ^{c}	924.08 ± 23.00 ^{a}	868.95 ± 9.24 ^{b}
Liver TNF-α (pg/mL)	321.94 ± 5.03 ^{c}	873.71 ± 38.52 ^{a}	482.97 ± 19.96 ^{b}
Liver MDA (nmol/mg prot)	0.78 ± 0.01 ^{c}	4.27 ± 0.10 ^{a}	2.39 ± 0.03 ^{b}
Liver CAT (U/mg prot)	33.42 ± 0.49 ^{a}	25.04 ± 0.47 ^{b}	33.65 ± 0.28 ^{a}
Liver SOD (U/mg prot)	6.29 ± 0.14 ^{a}	4.62 ± 0.04 ^{c}	5.86 ± 0.18 ^{b}
Liver GSH-Px (U/mg prot)	41.72 ± 1.29 ^{a}	18.79 ± 1.53 ^{c}	33.39 ± 1.93 ^{b}
Liver T-AOC (U/mg prot)	0.06 ± 0.001 ^{a}	0.04 ± 0.001 ^{c}	0.05 ± 0.002 ^{b}

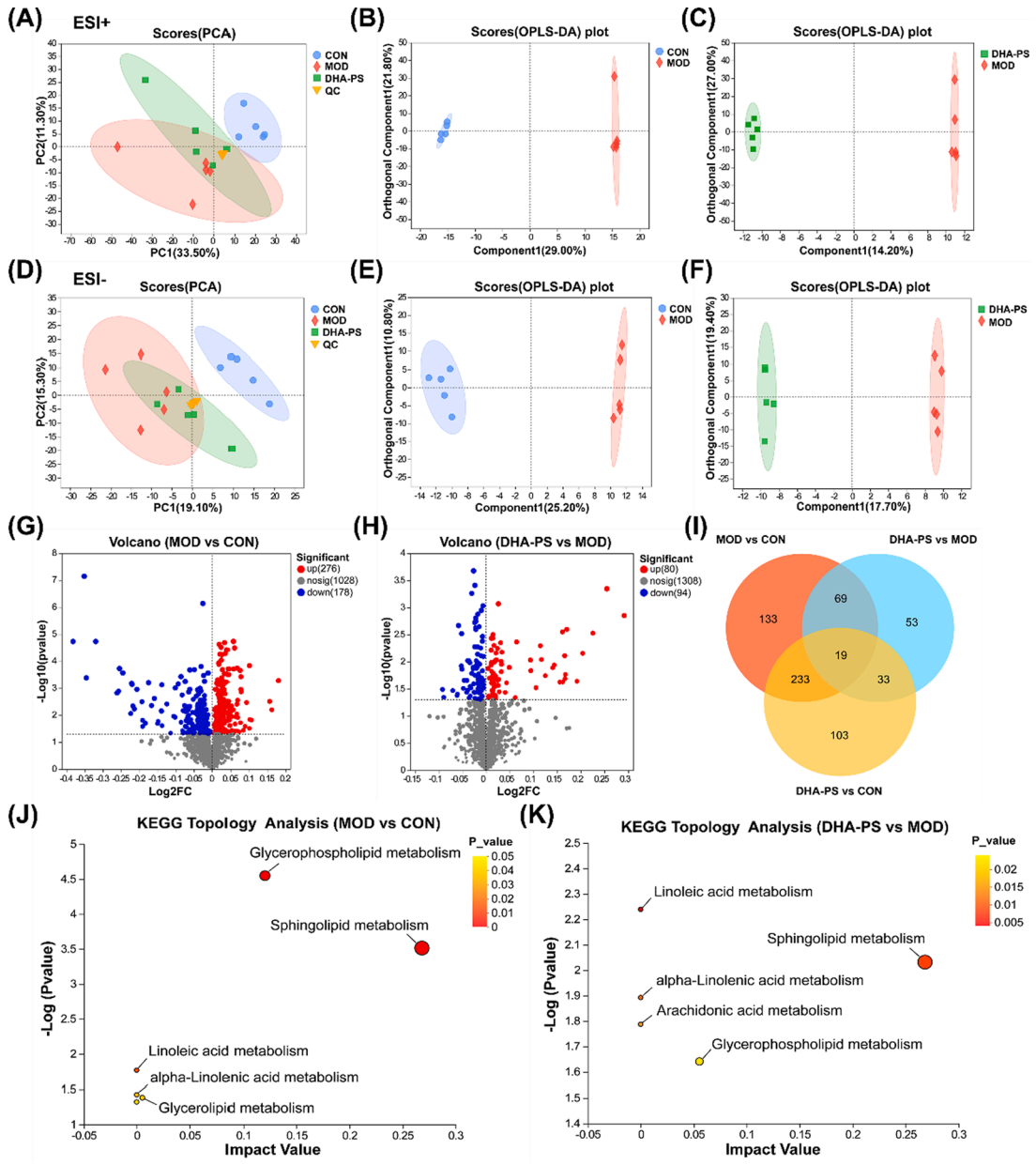

Fig. 2. The effect of DHA-PS on the metabolome profile of mice ($n = 5$). (A, D) PCA plot of positive ions and negative ions; (B, E) OPLS-DA plot of positive ions and negative ions (MOD *vs* CON); (C, F) OPLS-DA plot of positive ions and negative ions (DHA-PS *vs* MOD); (G) Volcano plot of MOD *vs* CON; (H) Volcano plot of DHA-PS *vs* MOD; (I) Venn diagram; (J, K) KEGG topological analysis of MOD *vs* CON comparison group and DHA-PS *vs* MOD comparison group.

displays 85 differential lipid metabolites shared between the MOD *vs* CON and DHA-PS *vs* MOD comparison groups, predominantly consisting of glycerolipids (GL), glycerophospholipids (GP), and sphingolipids (SP). We speculate that these differential metabolites are potential biomarkers for the dysregulation of hepatic lipid metabolism regulated by DHA-PS. Therefore, we further compared the changes in the levels of different lipids within GP, SP, and GL classes (Table. 2). Compared to the CON, significant increases were found in the MOD group for GP-associated lipids, such as PC (17:1/18:2), PC (19:0/18:2), PC (17:1/22:6), PE (15:0/18:2), PE (19:0/22:6), and in SP-associated lipids, such as Cer (d17:1/22:0), Cer (d18:2/22:2), Cer (d18:1/23:0), Cer (d18:1/25:3), Cer (t18:0/25:3), SM (t18:1/22:5), and in GL-associated lipids, such as DG (18:2e/20:4), TG (18:2/22:6/22:6) ($P < 0.05$), while a significant decrease was noted in LPC (20:1e) levels ($P < 0.05$). Interestingly, DHA-PS treatment reversed the aforementioned lipid level disorders. Additionally, KEGG pathway analysis of the selected differential lipid metabolites exhibited that the primary metabolic pathways affected in the MOD were sphingolipid metabolism and glycerophospholipid metabolism, with pathway impact values > 0.1 (Fig. 2J). The metabolic pathways affected by the DHA-PS group were also sphingolipid metabolism and glycerophospholipid metabolism, among which only sphingolipid metabolism had a pathway impact value > 0.1 (Fig. 2K). Therefore, we infer that DHA-PS could restore the lipid disorders induced by PS-NPs through modulating sphingolipid metabolism and glycerophosphatidylcholine metabolism in the liver, thereby regulating the normal operation of hepatic lipid metabolism.

3.4. Hepatic transcriptomic analysis

To further investigate how DHA-PS mitigates liver damage, transcriptomic studies were conducted to reveal differential gene expression in the liver after PS-NPs and DHA-PS treatment. Genes with a fold change ≥ 2 and $P < 0.05$ were considered as DEGs. Visualization of the changes in DEGs through volcano plots showed that compared to the

Table 2
Expression of representative differential lipid metabolites.

Differential lipid metabolites	CON	MOD	DHA-PS
LPC (20:1e)	(10.36 ± 2.30) × $10^{7\ a}$	(5.64 ± 1.47) × 10^{7c}	(8.01 ± 0.92) × 10^{7b}
PC (17:1/18:2)	(73.54 ± 6.36) × 10^{7c}	(90.22 ± 5.39) × $10^{7\ a}$	(80.39 ± 2.28) × 10^{7b}
PC (19:0/18:2)	(49.28 ± 5.09) × 10^{7c}	(77.93 ± 6.33) × $10^{7\ a}$	(62.74 ± 7.29) × 10^{7b}
PC (17:1/22:6)	(3.50 ± 0.68) × 10^{7c}	(6.25 ± 0.55) × $10^{7\ a}$	(4.63 ± 0.82) × 10^{7b}
PE (15:0/18:2)	(1.00 ± 0.14) × 10^{7b}	(1.36 ± 0.15) × $10^{7\ a}$	(1.07 ± 0.22) × 10^{7b}
PE (19:0/22:6)	(10.41 ± 0.59) × 10^{7c}	(14.41 ± 1.57) × $10^{7\ a}$	(12.44 ± 1.79) × 10^{7b}
Cer (d17:1/22:0)	(60.31 ± 7.32) × 10^{7b}	(81.52 ± 9.52) × $10^{7\ a}$	(61.88 ± 8.92) × 10^{7b}
Cer (d18:2/22:2)	(27.33 ± 2.73) × 10^{7b}	(34.00 ± 3.21) × $10^{7\ a}$	(29.51 ± 2.78) × 10^{7b}
Cer (d18:1/23:0)	(24.90 ± 4.39) × 10^{8b}	(36.13 ± 3.45) × $10^{8\ a}$	(28.29 ± 3.79) × 10^{8b}
Cer (d18:1/25:3)	(26.14 ± 4.48) × 10^{8b}	(34.35 ± 3.94) × $10^{8\ a}$	(26.67 ± 3.08) × 10^{8b}
Cer (t18:0/25:3)	(25.67 ± 4.40) × 10^{8b}	(33.71 ± 3.87) × $10^{8\ a}$	(26.19 ± 3.03) × 10^{8b}
SM (t18:1/22:5)	(0.80 ± 0.21) × 10^{7b}	(1.17 ± 0.23) × $10^{7\ a}$	(0.71 ± 0.23) × 10^{7b}
DG (18:2e/20:4)	(3.37 ± 2.12) × 10^{7b}	(7.21 ± 1.22) × $10^{7\ a}$	(4.43 ± 1.72) × 10^{7b}
TG (18:2/22:6/22:6)	(49.83 ± 9.05) × 10^{7b}	(73.35 ± 19.41) × $10^{7\ a}$	(53.00 ± 4.52) × 10^{7b}

CON, there were 63 genes significantly up-regulated and 386 genes significantly down-regulated in the MOD (Fig. 3A). In comparison with the MOD, the DHA-PS group exhibited 90 genes notably up-regulated and 40 genes notably down-regulated (Fig. 3B). GO enrichment analysis was conducted to better understand the biological functions of DEGs among different comparison groups, including Biological Process (BP), Molecular Function (MF), and Cellular Component (CC). In the MOD *vs* CON comparison group, DEGs were mainly enriched in BP categories such as lipid transport, positive regulation of protein phosphorylation, and response to endogenous stimulus (Fig. 3C). DEGs in the DHA-PS *vs* MOD comparison group were primarily enriched in BP categories, such as myeloid leukocyte migration, leukocyte chemotaxis, inflammatory response, and MF category Toll-like receptor 4 binding (Fig. 3D).

In addition, we performed KEGG pathway enrichment analysis on the DEGs from different treatment groups. As shown in Fig. 3E and F, the MOD *vs* CON comparison group was mainly enriched in pathways, such as the PI3K-Akt, TGF-beta, NOD-like receptor, MAPK, and lipid and atherosclerosis. On the other hand, the DHA-PS *vs* MOD comparison group was predominantly enriched in pathways including the IL-17, NOD-like receptor, TNF, lipid metabolism-related pathways associated with atherosclerosis, NF-κB, TLR, and inflammation mediators regulation of TRP channels. These findings suggest that the DEGs are predominantly linked to lipid metabolism processes and the the occurrence of inflammation.

3.5. Effect of DHA-PS on the SIRT1-AMPK and TLR4/NF-κB pathways

Long-term exposure to PS-NPs notably decreased the expression levels of SIRT1, AMPKα, and the lipolytic factor PPARα in the mouse liver, while the expression level of the lipogenic factor SREBP-1c notably increased (Fig. 4A, $P < 0.05$). However, DHA-PS intervention was able to reverse the changes in these measures. Compared with the CON, the levels of TLR4, p-P65/P65, and p-IκBα/IκBα in the MOD notably increased ($P < 0.05$). After gavage with DHA-PS, the ratios of TLR4 level (0.74 ± 0.02 *vs* 0.87 ± 0.05), p-P65/P65 (0.59 ± 0.01 *vs* 0.85 ± 0.10), and p-IκBα/IκBα (0.97 ± 0.19 *vs* 1.33 ± 0.14) decreased notably compared to the MOD (Fig. 4B, $P < 0.05$). Overall, DHA-PS can improve lipid metabolism disorders and reduce inflammation by stimulating the SIRT1-AMPK pathway, and suppressing the TLR4/NF-κB pathway.

3.6. DHA-PS enhances intestinal barrier function

To further explore the protective role of DHA-PS against intestinal barrier damage induced by PS-NPs, we examined the morphological alterations in mouse jejunum tissues using H&E staining. As illustrated in Fig. 5A, the jejunum villi in the CON were well-preserved and tightly organized, featuring intact epithelial cells. Conversely, the jejunum in the MOD displayed structural disorganization, characterized by villous atrophy and epithelial cell deterioration and loss, which resulted in a reduced villus-to-crypt ratio. The administration of DHA-PS progressively ameliorated the architecture of the mouse jejunum tissue. In addition, the expression levels of ZO-1, Occludin, and Claudin-1 in the MOD were significantly decreased compared to the CON ($P < 0.05$), indicating that exposure to PS-NPs disrupts the integrity of the intestinal mucosal barrier (Fig. 5B–E). In contrast, the expression levels of tight junction proteins (TJs) in the DHA-PS treatment group were notably enhanced ($P < 0.05$), suggesting that DHA-PS may enhance intestinal barrier function by up-regulating the expression levels of jejunum TJs.

3.7. Intestinal microbiota analysis

We assessed the effects of PS-NPs exposure and DHA-PS supplementation on the intestinal microbiota, observing that the rarefaction curve plateaued at higher sequencing depths, suggesting adequate sequencing coverage (Fig. 6A). The Venn diagram illustrated the common or unique OTUs among different groups (Fig. 6B), with 44, 57, and 105 unique OTUs in the CON, MOD, and DHA-PS groups, respectively, and a total of 454 OTUs shared among the three groups. We utilized α diversity analysis to evaluate the diversity and richness of the intestinal microbial community (Fig. 6D–G). Compared to the CON, the Shannon, Ace, and Chao indices decreased, while the Simpson index increased in the MOD. However, supplementation with DHA-PS restored these indices, indicating that DHA-PS can improve the decreased diversity and richness of the intestinal microbial community caused by PS-NPs. β diversity reflected overall structural changes in the microbial communities among groups, as revealed by principal coordinate analysis (PCoA) (Fig. 6C). There was evident separation among the CON, MOD, and DHA-PS groups, showing significant changes in the intestinal microbiota structure after different treatments. Moreover, the projection distance of the DHA-PS group along the horizontal axis was closer to the CON, indicating that DHA-PS partially regulated the changes in the microbial community structure.

To further determine the effects of PS-NPs and DHA-PS treatments on the gut microbiota, the composition of the microbial community was examined at the phylum and genus levels. At the phylum level, the predominant phyla detected included *Bacteroidota*, *Firmicutes*, *Verrucomicrobiota*, and *Actinobacteriota*, with *Bacteroidota* and *Firmicutes* being the most abundant (Fig. 6H). Compared to the CON, PS-NPs exposure increased the relative abundance of *Firmicutes* and *Actinobacteriota* while decreasing the relative abundance of *Bacteroidota* and *Verrucomicrobiota*, leading to a significant increase in the *Firmicutes/Bacteroidota* (F/B) ratio (1.19 ± 0.11 *vs* 0.83 ± 0.16, $P < 0.05$). However, supplementation with DHA-PS restored the changes in microbial abundance induced by PS-NPs, with the relative abundance of *Bacteroidota* increasing to 59.36 %, *Firmicutes* decreasing to 35.12 %, and the F/B ratio decreasing to 0.59 ± 0.11 (Fig. 6J). At the genus level, primarily detected were *norank_f_Muribaculaceae*, *Lactobacillus*, *Akkermansia*, *norank_f_norank_o_Clostridia_UCG-014*, and *Lachnospiraceae_NK4A136_group*. The relative abundances of *norank_f_Muribaculaceae*, *Akkermansia*, and *norank_f_norank_o_Clostridia_UCG-014* were decreased in the MOD compared to the CON, while *Lactobacillus* and *Lachnospiraceae_NK4A136_group* showed increased relative abundances (Fig. 6I). However, DHA-PS reversed the changes in relative abundances of the

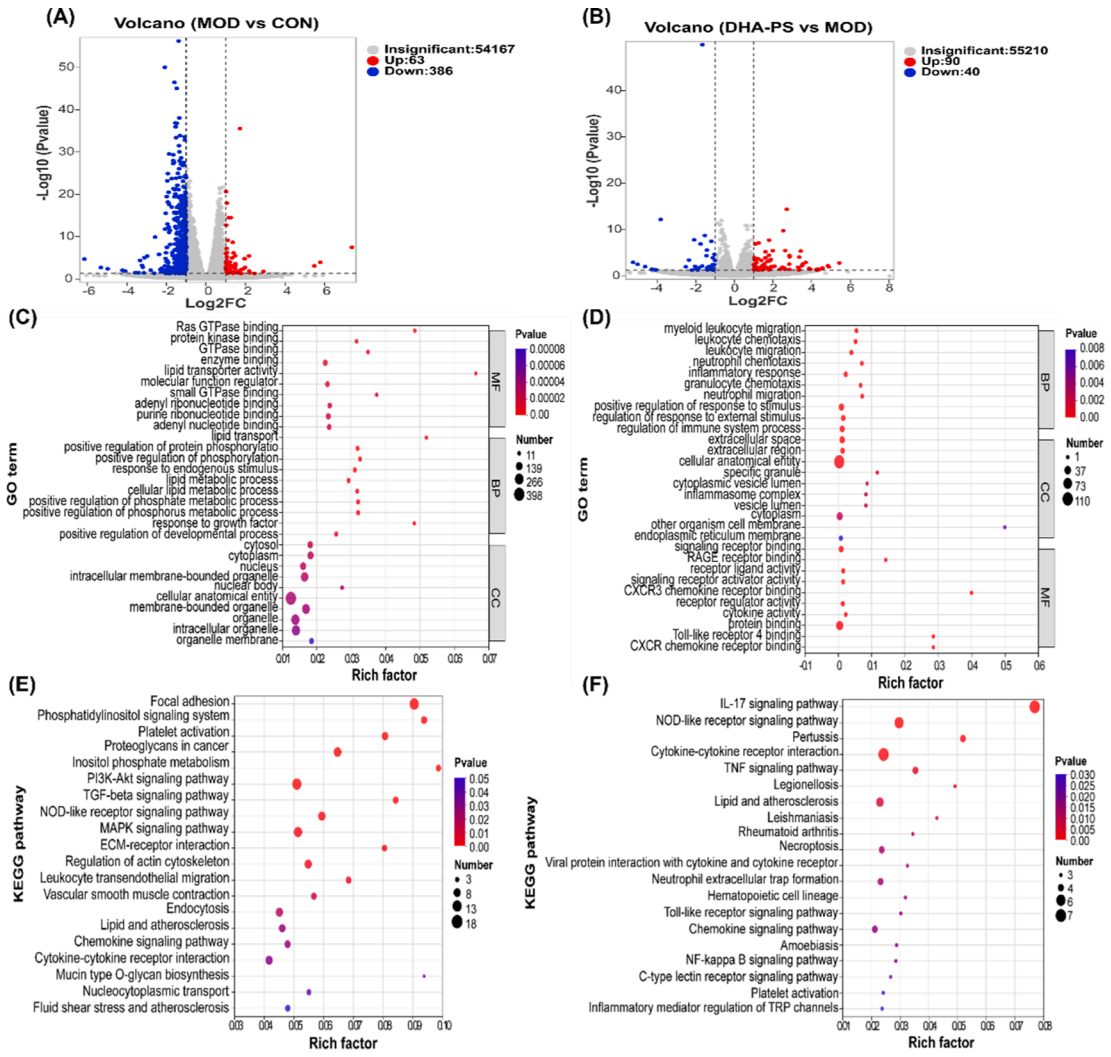

Fig. 3. The effect of DHA-PS on differential gene expression in mouse liver. (A, B) Volcano plots of DEGs in the MOD *vs* CON comparison group and the DHA-PS *vs* MOD comparison group. (C, D) Bubble plots of GO enrichment analysis for DEGs in the MOD *vs* CON comparison group and the DHA-PS *vs* MOD comparison group. (E, F) Bubble plots of KEGG pathway enrichment analysis for DEGs in the MOD *vs* CON comparison group and the DHA-PS *vs* MOD comparison group.

above genera. Furthermore, differential genera at the genus level were analyzed using Kruskal-Wallis rank-sum tests. As shown in Fig. 6K, the relative abundances of *Akkermansia* and *Parasutterella* decreased in the MOD, while those of *Coriobacteriaceae_UCG-002*, *Desulfovibrio*, and *Eubacterium_siraeum_group* increased. Supplementation with DHA-PS ameliorated the imbalance of these genera. As described above, DHA-PS effectively modulates the gut microbiota imbalance induced by exposure to PS-NPs at the phylum and genus levels.

The LEFSe analysis was employed to further identify microbial taxa contributing significantly to inter-group differences (LDA $\geq$ 3). As illustrated in Fig. 6L and M, 10, 9, and 9 taxa were enriched in the CON, MOD, and DHA-PS groups, respectively. In the CON, significantly enriched taxa included *Akkermansia*, *Parasutterella*, and *Sutterellaceae*. The predominant differential taxa in the MOD comprised *Atopobiaceae*, *Coriobacteriaceae_UCG-002*, *Paludicola*, and *Desulfovibrio*, while *Prevotellaceae*, *Intestinimonas*, *Alloprevotella*, and *Bacteroides* were predominant in the DHA-PS group.

3.8. Correlation analysis

Spearman correlation coefficients were calculated with a threshold of $|r| > 0.8$ and $P < 0.05$ to investigate the correlation among gut microbiota, liver biochemical indices, and differentially expressed liver lipid metabolites. The results, as shown in Fig. 7, indicate that *Desulfovibrio* is positively correlated with liver IL-1β, TNF-α, and PE (15:0/18:2). Both *Desulfovibrio* and *Coriobacteriaceae_UCG-002* are negatively correlated with liver CAT. *norank_f_Muribaculaceae* is positively correlated with liver CAT but negatively correlated with PE (15:0/18:2). *Akkermansia* and *norank_f_norank_o_Clostridia_UCG-014* are both positively correlated with liver GSH-Px but negatively correlated with liver TNF-α and DG (18:2e/20:4). Furthermore, liver NEFA, LPS, IL-6, PE (15:0/18:2), and Cer (d17:1/22:0) are all negatively correlated with *norank_f_norank_o_Clostridia_UCG-014*. These results suggest that the improvement in liver biochemical indices after DHA-PS supplementation is related with changes in gut microbiota and liver lipid metabolites.

4. Discussion

Humans are almost constantly exposed to low concentrations of NPs in the environment, and NPs can be ingested by humans through diet, respiration, and skin contact, accumulating in multiple organs such as the liver, kidneys, lungs, and intestines, thereby increasing health risks [26,27]. This study focuses on PS-NPs (100 nm) to evaluate their toxic effects on the liver and intestine. Consistent with previous studies [28,29], after prolonged exposure to PS-NPs, the liver index of mice significantly increased, and resulted in elevated serum transaminase

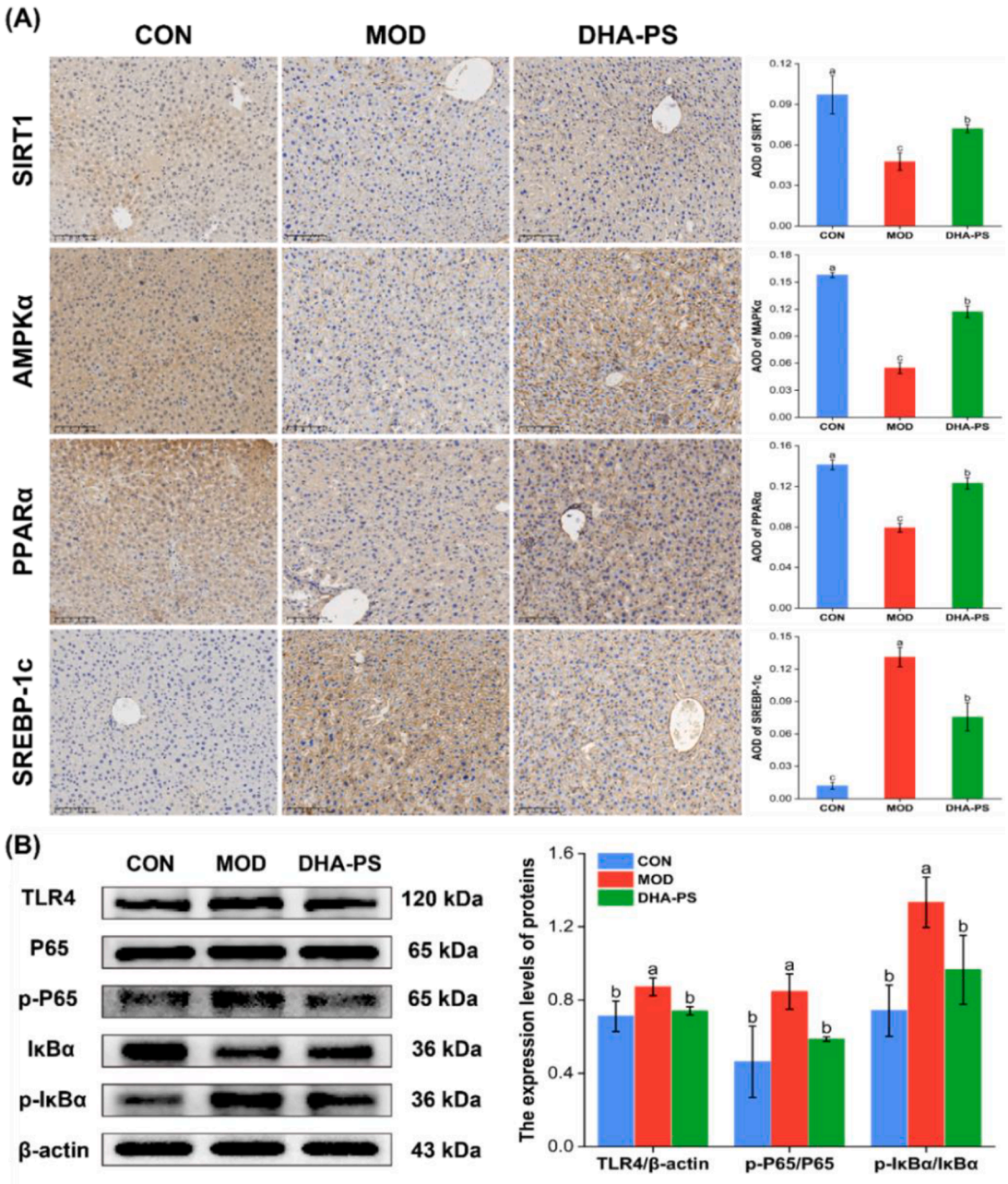

Fig. 4. The effects of DHA-PS on the SIRT1-AMPK and TLR4/NF-κB pathways ($n = 3$). (A) Immunohistochemical analysis of SIRT1, AMPKα, PPARα, and SREBP-1c (200×; scale bar: 100 μm); (B) Western blotting of TLR4/β-actin, p-P65/P65, p-IκBα/IκBα proteins.

levels, accompanied by disordered hepatic cord arrangement and vacuolar degeneration. This suggests that long-term exposure to PS-NPs can cause liver damage. However, supplementation with DHA-PS not only restored liver metabolic function but also improved the damage to the morphology of liver tissue, suggesting that DHA-PS can effectively ameliorate liver damage induced by PS-NPs in mice.

Oxidative stress and inflammatory response are considered potential mechanisms underlying the hepatotoxicity induced by PS-NPs [30]. PS-NPs treatment could lead to a notable increase in ROS concentration and Nrf2 expression in the mouse liver, accompanied by elevated levels of inflammatory response proteins and inflammatory cytokines mRNA [31]. In this study, PS-NPs inhibited the CAT, SOD, GSH-Px, and T-AOC activities in the mouse liver and enhanced the MDA content, which was similar to previous findings [32]. It has been reported that oxidative stress can accelerate the development of inflammation by increasing the accumulation of inflammatory cells and the expression of proinflammatory cytokines in tissues [33]. Furthermore, liver inflammation commonly accompanies chronic liver disease, frequently linked with heightened liver exposure to LPS [34]. Our findings revealed that PS-NPs substantially elevated the serum and hepatic LPS levels and increased the levels of TNF-α, IL-6, and IL-1β in the liver while decreasing IL-10 levels. This suggests that PS-NPs enhance the release of pro-inflammatory cytokines triggered by LPS, thereby intensifying liver inflammation. Conversely, supplementation with DHA-PS effectively mitigated liver damage induced by PS-NPs by enhancing antioxidant capabilities and suppressing inflammatory responses.

Previous research has shown that NPs deposited in the liver promote lipid accumulation and accelerate the destruction of normal lipid metabolism in the liver [35]. In this study, the lipid levels (TC, TG, and NEFA) in the MOD were significantly elevated, with severe lipid droplet accumulation. Additionally, SIRT1 and AMPK, as energy sensors within cells, play important roles in coordinating metabolism and energy

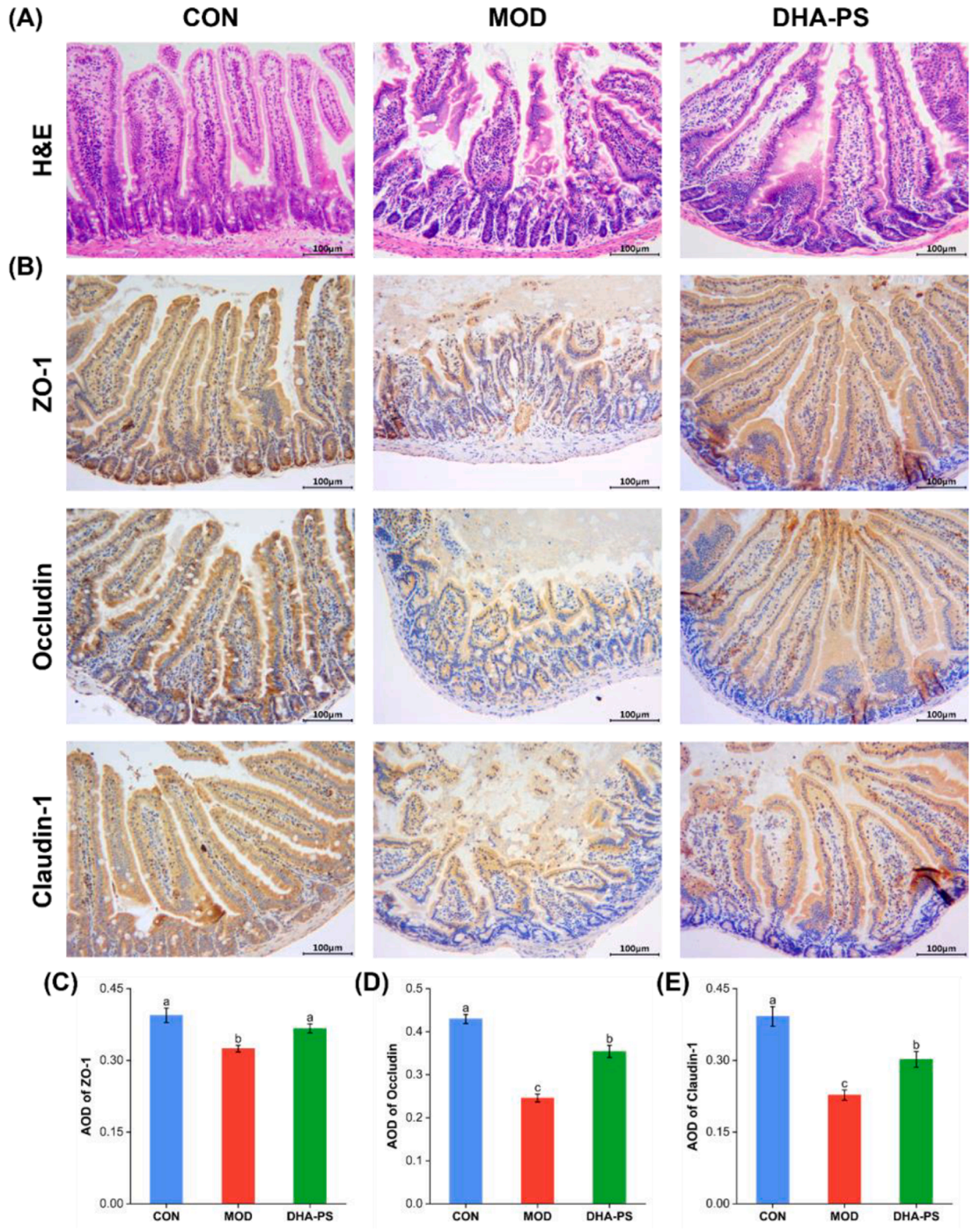

Fig. 5. The effect of DHA-PS on the morphology of mouse jejunum tissue and TJs. (A) Jejunum H&E staining (200×; scale bar 100 μm); (B) Immunohistochemical analysis (200×; scale bar 100 μm); (C) AOD of ZO-1; (D) AOD of Occludin; (E) AOD of Claudin-1.

balance [36]. PPARα is a key factor controlling fatty acid β-oxidation, while SREBP1 is an important regulatory factor in lipid synthesis [37]. Previous research has found associations between exposure to MPs and down-regulation of SIRT1, AMPK, and PPARα expression, as well as upregulation of SREBP-1 expression [38]. Lai *et al.* [38] found that PS-NPs induced excessive lipid accumulation in the liver of *Larimichthys crocea* by down-regulating the expression of PPARα, a protein related to lipid catabolism, and inhibiting the AMPK-PPARα signaling pathway. Our study found similar results, the expression levels of SIRT1, AMPKα, and PPARα in the mouse liver notably decreased, while the expression level of SREBP-1c notably increased after PS-NPs exposure. These results collectively indicate that long-term exposure to PS-NPs inhibits the SIRT1-AMPK pathway, exacerbating lipid accumulation in the liver and affecting liver lipid metabolism. Following DHA-PS treatment, the expression levels of the above factors and the accumulation of lipids were significantly improved.

Lipid metabolism is a highly complex process, and lipid molecules play crucial roles in keeping biological functions and cellular integrity, as well as participating in the pathogenesis of diseases [39]. Here, we conducted a lipidomic analysis of mouse liver to further elucidate the lipid changes after PS-NPs exposure and the beneficial effects of DHA-PS. It is noteworthy that sphingolipid metabolism and glycerophospholipid metabolism are the most important pathways. Besides their role in forming biological membranes, glycerophospholipids

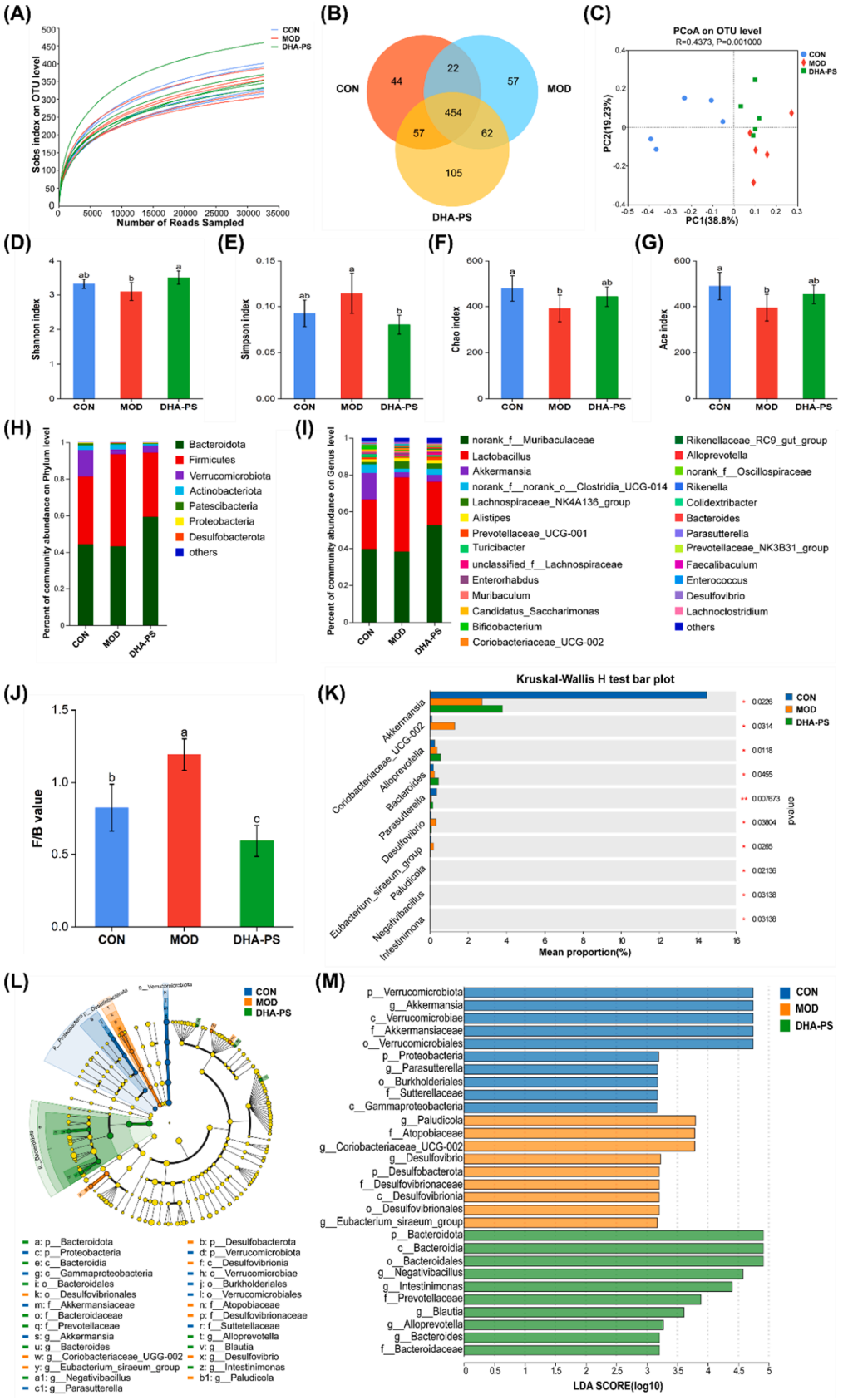

Fig. 6. The effects of DHA-PS on the gut microbiota of mice ($n = 5$). (A) Rarefaction curve; (B) Venn diagram; (C) PCoA analysis; (D) Shannon index; (E) Simpson index; (F) Chao index; (G) Ace index; (H) Species composition at the phylum level; (I) Species composition at the genus level; (J) F/B ratio; (K) Kruskal-Wallis rank-sum test; (L) LEfSe cladogram; (M) LDA histogram.

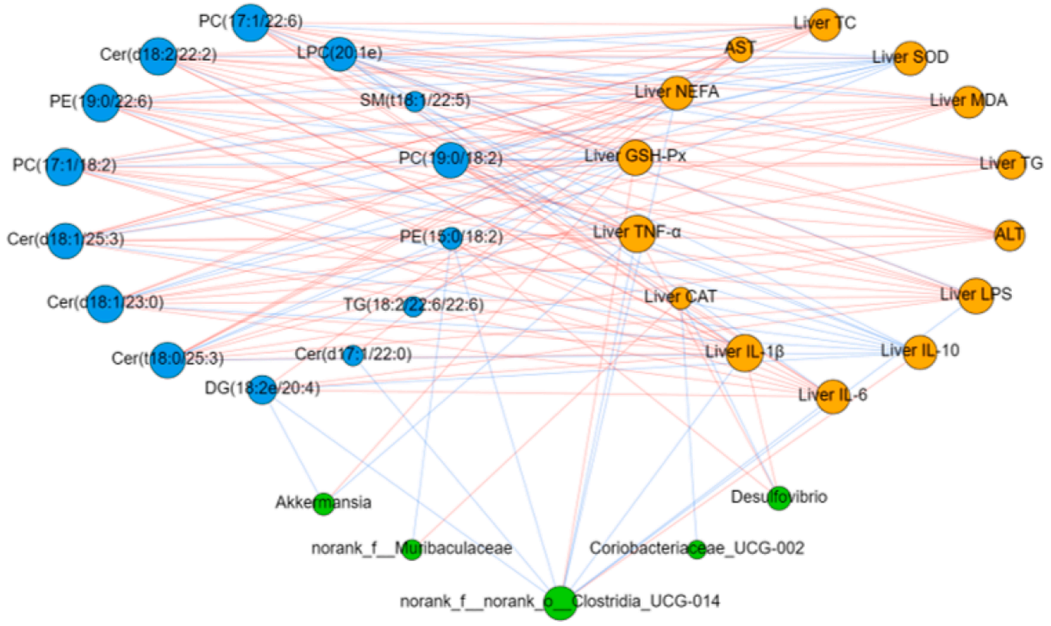

Fig. 7. Spearman correlation network diagram. red indicates positive correlation, while blue indicates negative correlation.

participate in a range of physiological activities including inflammatory responses, cellular metabolism, and signal transduction [40]. Among them, PC and PE are the most abundant lipid classes in mammalian cells, playing important roles in membrane repair and cellular homeostasis. However, abnormally elevated levels of PC can promote TG synthesis, leading to lipid accumulation [41]. Lysophosphatidylcholine (LPC) is a hydrolyzed product of PC by the action of phospholipase A2, and its downregulated levels can accelerate hepatic fatty acid oxidation, induce hepatic oxidative stress, enhance inflammatory responses, and cause cytotoxicity [42]. Our study showed that PS-NPs significantly enhanced the levels of PC (17:1/18:2), PC (19:0/18:2), PC (17:1/22:6), PE (15:0/18:2), and PE (19:0/22:6), as well as the content of DG (18:2e/20:4) and TG (18:2/22:6/22:6), while significantly reducing the level of LPC (20:1e). Additionally, ceramides (Cer) and sphingomyelins (SM) serve as core products of sphingolipid metabolism and are the most abundant sphingolipids in mammalian cells, capable of activating the TLR4/NF-κB pathway, thereby increasing the secretion of pro-inflammatory cytokines [43]. In our study, compared to the CON, the levels of Cer and SM in the MOD were notably up-regulated. DHA-PS administration restored the levels of various sphingolipids and glycerophospholipids to normal levels, indicating that DHA-PS can improve PS-NPs-induced disruption of lipid metabolism in mouse livers by regulating glycerophospholipid metabolism and sphingolipid metabolism.

The noteworthy observation from the transcriptomic sequencing results is that the DEGs between the DHA-PS and MOD comparison groups mainly involve inflammatory pathways, such as the TLR pathway and NF-κB pathway. This precisely indicates the close relationship between lipid metabolism disorders and inflammatory responses. TLRs participate in the non-specific immune response of the body [44]. TLR4, as one of the family members of toll-like receptors, can effectively regulate the transcription, translation, and expression of apoptotic proteins to regulate the inflammatory process [45]. NF-κB is the downstream target gene of TLR4, which can enter the nucleus once activated and participate in the regulation of pro-inflammatory and immune responses [46]. Chen *et al.* [47] showed that oral administration of PS-NPs activated the TLR4/NF-κB/NLRP3/GSDMD pathway, causing intestinal and liver inflammation and hepatocyte pyroptosis. Zhang et al. [48] found that PS-MPs exposure significantly increased the expression of TLR4 pathway-related factors in carp. Similar to their results, in this study, PS-NPs exposure significantly up-regulated the expression of TLR4 and activated the downstream NF-κB pathway, thereby inducing inflammation in the mouse liver. DHA-PS can inhibit the TLR4/NF-κB pathway by down-regulating the expression of TLR4 and the ratio of p-IκBα/IκBα and p-P65/P65.

The intestine is a complex barrier exchange system and the most important pathway for nutrients and toxic substances to enter the body [49]. Animal experiments indicate that orally ingested NPs first aggregate in the intestine, then pass through the intestinal barrier to be transported to the mesenteric blood vessels, ultimately entering the bloodstream [50]. Moreover, increasing evidence suggests that the continuous accumulation of NPs in the intestine can cause varying degrees of intestinal toxicity [51]. Histopathological examination also found that PS-NPs caused villous atrophy and epithelial cell shedding in the jejunum. TJs are the main adhesion molecules between intestinal mucosal epithelial cells, crucial for maintaining intestinal epithelial barrier function and absorption of nutrients [52]. Li *et al.* [53] demonstrated that exposure to PS-NPs reduced the expression of TJs in intestinal tissue. Consistent with our findings, immunohistochemistry of the jejunum exhibited a notable decrease in the expression levels of TJs in the MOD. Following DHA-PS intervention, these indicators were all reversed, suggesting that DHA-PS can alleviate intestinal barrier damage caused by PS-NPs.

The gut microbiota plays critical roles in digestion, absorption, immune responses, and intestinal barrier function, closely linked to host health [54,55]. Reports suggest that upon entering the intestine, NPs first interact with the gut microbiota, influencing its composition and function [56]. When the dynamic equilibrium between beneficial and harmful bacteria in the gut microbiota is disturbed, it can result in infections and various liver disorders [57,58]. Our results indicate that PS-NPs reduce the relative abundance of beneficial gut bacteria *norank_f_Muribaculaceae*, *Akkermansia*, and *norank_f_norank_o_Clostridia_UCG-014*, while increasing the relative abundance of pathogenic gut bacteria *Coriobacteriaceae_UCG-002* and *Desulfovibrio*. According to reports, *norank_f_Muribaculaceae* is a symbiotic bacterium in the intestine, known to promote the production of SCFAs and improve intestinal inflammatory responses and damage [59]. *Norank_f_norank_o_Clostridia_UCG-014* can regulate lipid metabolism disorder and has been shown to decrease in mice with colitis induced by dextran sulfate sodium (DSS) [60]. Additionally, the lack or decreased abundance of *Akkermansia* is related with various diseases such as obesity, hepatic

steatosis, and inflammatory bowel disease [61]. Bian *et al.* [40] found that gavage with *Akkermansia* in a DSS-induced colitis mouse model could alleviate mucosal inflammation, protect the intestinal barrier, and decrease the level of inflammatory factors in the intestine. Therefore, we speculate that the relative decrease in the abundance of *norank_f_Muribaculaceae*, *norank_f_norank_o_Clostridia_UCG-014*, and *Akkermansia* in MOD group mice is one of the important factors leading to intestinal barrier dysfunction. Research indicates that *Desulfovibrio* has the ability to reduce sulfate, and the hydrogen sulfide it produces can damage intestinal epithelial cells and promote intestinal inflammation [62]. This is highly similar to the increase in inflammatory factor levels and the relative abundance of *Desulfovibrio* observed in this study. Additionally, *Coriobacteriaceae_UCG-002* belongs to the Coriobacteriaceae family, and its production of phenol and cresol is cytotoxic and can reduce intestinal barrier function [63]. Yu *et al.* [64] also confirmed in their study that the increase in the abundance of *Coriobacteriaceae_UCG-002* and *Desulfovibrio* promotes intestinal inflammation and epithelial permeability. Overall, DHA-PS regulates intestinal dysbiosis by up-regulating the abundance of beneficial bacteria and down-regulating the abundance of pathogenic bacteria, thereby improving hepatotoxicity induced by PS-NPs through the "gut-liver axis".

5. Conclusion

In conclusion, exposure to PS-NPs can induce murine hepatotoxicity, and supplementation of DHA-PS ameliorates this damage, primarily by reducing liver lipid accumulation, inflammatory responses, and oxidative stress. It also modulates pathways related to sphingoid metabolism, glycerophospholipid metabolism, and the SIRT1/AMPK and TLR4/NF-κB. Furthermore, DHA-PS enhances the intestinal mucosal barrier function and modulates the gut microbiota, thereby improving PS-NPs-induced murine intestinal injury. This study comprehensively examines the beneficial effects and underlying mechanisms of DHA-PS on PS-NPs-induced hepatotoxicity in mice, providing a scientific rationale for the potential use of DHA-PS as a dietary supplement.

CRediT authorship contribution statement

Yuanlei Zhang: Writing – original draft, Methodology, Investigation. **Qiaoling Zhao:** Funding acquisition, Formal analysis, Data curation. **Rui Zhao:** Methodology, Investigation, Formal analysis, Data curation. **Yun Lu:** Formal analysis, Data curation. **Su Jiang:** Formal analysis, Data curation. **Yun-ping Tang:** Writing – review & editing, Funding acquisition, Conceptualization.

Declaration of competing interest

The authors declare that they have no known competing financial interests or personal relationships that could have appeared to influence the work reported in this paper.

Data availability

Data will be made available on request.

Acknowledgments

This work was financially supported by the Zhejiang Provincial Natural Science Foundation of China (No. LTGD23D060001), and the Eyas Program Incubation Project of Zhejiang Provincial Administration for Market Regulation (No. CY2023329).

Appendix A. Supplementary data

Supplementary data to this article can be found in Fig. S1: Permutation plots; Fig. S2: Cluster heatmap of 85 representative differential lipid metabolites in common; Table S1: The 85 representative differential lipid metabolites in common (VIP > 1, $P < 0.05$). Supplementary data to this article can be found online at https://doi.org/10.1016/j.intimp.2024.113154.

References

[1] W. Cai, L.A. Tremblay, L. An, Enhancing consumption responsibility to address global plastic pollution, Mar. Pollut. Bull. 183 (2022) 114089.
[2] H. Tong, X. Zhong, Z. Duan, X. Yi, F. Cheng, W. Xu, X. Yang, Micro- and nanoplastics released from biodegradable and conventional plastics during degradation: formation, aging factors, and toxicity, Sci. Total Environ. 833 (2022) 155275.
[3] J.-L. Xu, X. Lin, J.J. Wang, A.A. Gowen, A review of potential human health impacts of micro- and nanoplastics exposure, Sci. Total Environ. 851 (Pt 1) (2022) 158111.
[4] H.A. Leslie, M.J.M. van Velzen, S.H. Brandsma, A.D. Vethaak, J.J. Garcia-Vallejo, M.H. Lamoree, Discovery and quantification of plastic particle pollution in human blood, Environ. Int. 163 (2022) 107199.
[5] S. Fraissinet, G.E. De Benedetto, C. Malitesta, R. Holzinger, D. Materić, Microplastics and nanoplastics size distribution in farmed mussel tissues, Commun. Earth Environ. 5 (1) (2024) 128.
[6] Y. Lee, S. Cho, K. Park, T. Kim, J. Kim, D.-Y. Ryu, J. Hong, Potential lifetime effects caused by cellular uptake of nanoplastics: a review, Environ. Pollut. 329 (2023) 121668.
[7] T. Atugoda, H. Piyumali, H. Wijesekara, C. Sonne, S.S. Lam, K. Mahatantila, M. Vithanage, Nanoplastic occurrence, transformation and toxicity: a review, Environ. Chem. Lett. 21 (1) (2023) 363–381.
[8] X. Qian, P. Jin, K. Fan, H. Pei, Z. He, R. Du, C. Cao, Y. Yang, Polystyrene microplastics exposure aggravates acute liver injury by promoting Kupffer cell pyroptosis, Int. Immunopharmacol. 126 (2024) 111307.
[9] Z. Hou, R. Meng, G. Chen, T. Lai, R. Qing, S. Hao, J. Deng, B. Wang, Distinct accumulation of nanoplastics in human intestinal organoids, Sci. Total Environ. 838 (Pt 2) (2022) 155811.
[10] S. Sangkham, O. Faikhaw, N. Munkong, P. Sakunkoo, C. Arunlertaree, M. Chavali, M. Mousazadeh, A. Tiwari, A review on microplastics and nanoplastics in the environment: their occurrence, exposure routes, toxic studies, and potential effects on human health, Mar. Pollut. Bull. 181 (2022) 113832.
[11] S. Haldar, N. Yhome, Y. Muralidaran, S. Rajagopal, P. Mishra, Nanoplastics toxicity specific to liver in inducing metabolic dysfunction-a comprehensive review, Genes 14 (3) (2023) 590.
[12] C. Shi, X. Han, W. Guo, Q. Wu, X. Yang, Y. Wang, G. Tang, S. Wang, Z. Wang, Y. Liu, M. Li, M. Lv, Y. Guo, Z. Li, J. Li, J. Shi, G. Qu, G. Jiang, Disturbed Gut-Liver axis indicating oral exposure to polystyrene microplastic potentially increases the risk of insulin resistance, Environ. Int. 164 (2022) 107273.
[13] K. Yin, D. Wang, Y. Zhang, H. Lu, Y. Wang, M. Xing, Dose-effect of polystyrene microplastics on digestive toxicity in chickens (Gallus gallus): multi-omics reveals critical role of gut-liver axis, J. Adv. Res. 52 (2023) 3–18.
[14] H. Zhang, Y. Lu, Y. Zhang, J. Dong, S. Jiang, Y. Tang, DHA-enriched phosphatidylserine ameliorates cyclophosphamide-induced liver injury via regulating the gut-liver axis, Int. Immunopharmacol. 140 (2024) 112895.
[15] X. Wang, K. Deng, P. Zhang, Q. Chen, J.T. Magnuson, W. Qiu, Y. Zhou, Microplastic-mediated new mechanism of liver damage: From the perspective of the gut-liver axis, Sci. Total Environ. 919 (2024) 170962.
[16] O. Pabst, M.W. Hornef, F.G. Schaap, V. Cerovic, T. Clavel, T. Bruns, Gut–liver axis: barriers and functional circuits, Nat. Rev. Gastroenterol. Hepatol. 20 (7) (2023) 447–461.
[17] Y. Chen, H. Jin, F. Yang, S. Jin, C. Liu, L. Zhang, J. Huang, S. Wang, Z. Yan, X. Cai, R. Zhao, F. Yu, Z. Yang, G. Ding, Y. Tang, Physicochemical, antioxidant properties of giant croaker (Nibea japonica) swim bladders collagen and wound healing evaluation, Int. J. Biol. Macromol. 138 (2019) 483–491.
[18] Z. Wang, Y. Fang, Y. Zeng, X. Yang, F.-M. Yu, B. Wang, Immunomodulatory peptides from thick-shelled mussel (Mytilus coruscus): Isolation, identification, molecular docking and immunomodulatory effects on RAW264.7 cells, Food Biosci. 59 (2024) 103874.
[19] X. Huang, H. Wang, Z. Tu, A comprehensive review of the control and utilization of aquatic animal products by autolysis-based processes: mechanism, process, factors, and application, Food Res. Int. 164 (2023) 112325.
[20] M. Cretton, G. Malanga, T. Mazzuca Sobczuk, M. Mazzuca, Marine lipids as a source of high-quality fatty acids and antioxidants, Food Res. Int. 39 (8) (2023) 4941–4964.
[21] Y. Tang, R. Zhao, Q. Pu, S. Jiang, F. Yu, Z. Yang, T. Han, Investigation of nephrotoxicity on mice exposed to polystyrene nanoplastics and the potential amelioration effects of DHA-enriched phosphatidylserine, Sci. Total Environ. 892 (2023) 164808.
[22] T.-T. Zhang, J. Xu, Y.-M. Wang, C.-H. Xue, Health benefits of dietary marine DHA/EPA-enriched glycerophospholipids, Prog. Lipid. Res. 75 (2019) 100997.
[23] Y. Zhou, S. Tian, L. Qian, S. Jiang, Y. Tang, T. Han, DHA-enriched phosphatidylserine ameliorates non-alcoholic fatty liver disease and intestinal dysbacteriosis in mice induced by a high-fat diet, Food Funct. 12 (9) (2021) 4021–4033.
[24] H. Zhang, S. Tian, Q. Zhao, Y. Xu, L. Bi, S. Jiang, Y. Tang, Non-targeted metabolomics reveals a modulatory effect of DHA-enriched phosphatidylserine in

high fat-diet induced non-alcoholic fatty liver disease in mice, Process Biochem. 135 (2023) 22–32.
[25] Y. Jiang, L. Zhao, J. Ma, Y. Yang, B. Zhang, J. Xu, R. Dhondrup, T.W. Wong, D. Zhang, Preventive mechanisms of Chinese Tibetan medicine Triphala against nonalcoholic fatty liver disease, Phytomedicine 123 (2024) 155229.
[26] M.S. Yee, L.-W. Hii, C.K. Looi, W.-M. Lim, S.-F. Wong, Y.-Y. Kok, B.-K. Tan, C.-Y. Wong, C.-O. Leong, Impact of Microplastics and Nanoplastics on Human Health, Nanomaterials 11 (2) (2021) 496.
[27] M. Shen, Y. Zhang, Y. Zhu, B. Song, G. Zeng, D. Hu, X. Wen, X. Ren, Recent advances in toxicological research of nanoplastics in the environment: a review, Environ. Pollut. 252 (Pt A) (2019) 511–521.
[28] N.A.E. Yasin, M.E. El-Naggar, Z.S.O. Ahmed, M.K. Galal, M.M. Rashad, A. M. Youssef, E.M.M. Elleithy, Exposure to Polystyrene nanoparticles induces liver damage in rat via induction of oxidative stress and hepatocyte apoptosis, Environ. Toxicol. Pharmacol. 94 (2022) 103911.
[29] J. Ma, Y. Wan, L. Song, L. Wang, H. Wang, Y. Li, D. Huang, Polystyrene nanobeads exacerbate chronic colitis in mice involving in oxidative stress and hepatic lipid metabolism, Part. Fibre Toxicol. 20 (1) (2023) 49.
[30] Y. Wu, Y. Yao, H. Bai, K. Shimizu, R. Li, C. Zhang, Investigation of pulmonary toxicity evaluation on mice exposed to polystyrene nanoplastics: the potential protective role of the antioxidant N-acetylcysteine, Sci. Total Environ. 855 (2023) 158851.
[31] M. Panizzolo, V.H. Martins, F. Ghelli, G. Squillacioti, V. Bellisario, G. Garzaro, D. Bosio, N. Colombi, R. Bono, E. Bergamaschi, Biomarkers of oxidative stress, inflammation, and genotoxicity to assess exposure to micro- and nanoplastics. A literature review, Ecotox. Environ. Saf. 267 (2023) 115645.
[32] L. Li, M. Xu, C. He, H. Wang, Q. Hu, Polystyrene nanoplastics potentiate the development of hepatic fibrosis in high fat diet fed mice, Environ. Toxicol. 37 (2) (2022) 362–372.
[33] A. Banerjee, W.L. Shelver, Micro- and nanoplastic induced cellular toxicity in mammals: a review, Sci. Total Environ. 755 (Pt 2) (2021) 142518.
[34] X. Gu, M. Wei, F. Hu, H. Ouyang, Z. Huang, B. Lu, L. Ji, Chlorogenic acid ameliorated non-alcoholic steatohepatitis via alleviating hepatic inflammation initiated by LPS/TLR4/MyD88 signaling pathway, Chem. Biol. Interact. 376 (2023) 110461.
[35] H.T. Shiu, X. Pan, Q. Liu, K. Long, K.K.Y. Cheng, B.-C.-B. Ko, J.-K.-H. Fang, Y. Zhu, Dietary exposure to polystyrene nanoplastics impairs fasting-induced lipolysis in adipose tissue from high-fat diet fed mice, J. Hazard. Mater. 440 (2022) 129698.
[36] R.A.K. Srivastava, S.L. Pinkosky, S. Filippov, J.C. Hanselman, C.T. Cramer, R. S. Newton, AMP-activated protein kinase: an emerging drug target to regulate imbalances in lipid and carbohydrate metabolism to treat cardio-metabolic diseases: thematic review series: new lipid and lipoprotein targets for the treatment of cardiometabolic diseases, J. Lipid Res. 53 (12) (2012) 2490–2514.
[37] S. Rodriguez-Cuenca, V. Pellegrinelli, M. Campbell, M. Oresic, A. Vidal-Puig, Sphingolipids and glycerophospholipids - the "ying and yang" of lipotoxicity in metabolic diseases, Prog. Lipid. Res. 66 (2017) 14–29.
[38] W. Lai, D. Xu, J. Li, Z. Wang, Y. Ding, X. Wang, X. Li, N. Xu, K. Mai, Q. Ai, Dietary polystyrene nanoplastics exposure alters liver lipid metabolism and muscle nutritional quality in carnivorous marine fish large yellow croaker (Larimichthys crocea), J. Hazard. Mater. 419 (2021) 126454.
[39] Y. Zheng, X. Gan, C. Lin, D. Wang, R. Chen, Y. Dai, L. Jiang, C. Huang, Y. Zhu, Y. Song, J. Chen, Polystyrene nanoplastics cause reproductive toxicity in zebrafish: PPAR mediated lipid metabolism disorder, Sci. Total Environ. 931 (2024) 172795.
[40] L. Bian, H.-G. Chen, X.-J. Gong, C. Zhao, X. Zhou, Mori fructus polysaccharides attenuate alcohol-induced liver damage by regulating fatty acid synthesis, degradation and glycerophospholipid metabolism in mice, Front. Pharmacol. 12 (2021) 766737.
[41] W. Huang, P. Xie, Z. Cai, Lipid metabolism disorders contribute to hepatotoxicity of triclosan in mice, J. Hazard. Mater. 384 (2020) 121310.
[42] N. Tanaka, T. Matsubara, K.W. Krausz, A.D. Patterson, F.J. Gonzalez, Disruption of phospholipid and bile acid homeostasis in mice with nonalcoholic steatohepatitis, Hepatology 56 (1) (2012) 118–129.
[43] H. Sakamoto, T. Yoshida, T. Sanaki, S. Shigaki, H. Morita, M. Oyama, M. Mitsui, Y. Tanaka, T. Nakano, S. Mitsutake, Y. Igarashi, H. Takemoto, Possible roles of long-chain sphingomyelines and sphingomyelin synthase 2 in mouse macrophage inflammatory response, Biochem. Biophys. Res. Commun. 482 (2) (2017) 202–207.
[44] Q. Zhao, F. Yang, Q. Pu, R. Zhao, S. Jiang, Y. Tang, Integrative metabolomics and gut microbiota analyses reveal the protective effects of DHA-enriched phosphatidylserine on bisphenol A-induced intestinal damage, J. Funct. Foods 117 (2024) 106229.
[45] S. Tian, X. Jiang, Y. Tang, T. Han, Laminaria japonica fucoidan ameliorates cyclophosphamide-induced liver and kidney injury possibly by regulating Nrf2/HO-1 and TLR4/NF-κB signaling pathways, J. Sci. Food Agric. 102 (6) (2022) 2604–2612.
[46] S.-N. Chen, Y. Tan, X.-C. Xiao, Q. Li, Q. Wu, Y.-Y. Peng, J. Ren, M.-L. Dong, Deletion of TLR4 attenuates lipopolysaccharide-induced acute liver injury by inhibiting inflammation and apoptosis, Acta Pharmacol. Sin. 42 (10) (2021) 1610–1619.
[47] X. Chen, Y. Xuan, Y. Chen, F. Yang, M. Zhu, J. Xu, J. Chen, Polystyrene nanoplastics induce intestinal and hepatic inflammation through activation of NF-κB/NLRP3 pathways and related gut-liver axis in mice, Sci. Total Environ. 935 (2024) 173458.
[48] Q. Zhang, F. Wang, S. Xu, J. Cui, K. Li, X. Shiwen, M.-Y. Guo, Polystyrene microplastics induce myocardial inflammation and cell death via the TLR4/NF-κB pathway in carp, Fish Shellfish Immun. 135 (2023) 108690.
[49] M.H. Jin, J.N. Hu, M. Zhang, Z. Meng, G.P. Shi, Z. Wang, W. Li, Maltol attenuates polystyrene nanoplastic-induced enterotoxicity by promoting AMPK/mTOR/TFEB-mediated autophagy and modulating gut microbiota, Environ. Pollut. 322 (2023) 121202.
[50] S. Winzen, J.C. Schwabacher, J. Müller, K. Landfester, K. Mohr, Small surfactant concentration differences influence adsorption of human serum albumin on polystyrene nanoparticles, Biomacromolecules 17 (11) (2016) 3845–3851.
[51] Z. Li, L. Yan, M. Junaid, X. Chen, H. Liao, D. Gao, Q. Wang, Y. Zhang, J. Wang, Impacts of polystyrene nanoplastics at the environmentally relevant and sub-lethal concentrations on the oxidative stress, immune responses, and gut microbiota to grass carp (Ctenopharyngodon idella), J. Hazard. Mater. 441 (2023) 129995.
[52] K. Sun, Y. Lei, R. Wang, Z. Wu, G. Wu, Cinnamicaldehyde regulates the expression of tight junction proteins and amino acid transporters in intestinal porcine epithelial cells, J. Anim. Sci. Biotechnol. 8 (1) (2017) 66.
[53] L. Li, X. Lv, J. He, L. Zhang, B. Li, X. Zhang, S. Liu, Y. Zhang, Chronic exposure to polystyrene nanoplastics induces intestinal mechanical and immune barrier dysfunction in mice, Ecotox. Environ. Saf. 269 (2024) 115749.
[54] N. Li, J. Wang, P. Liu, J. Li, C. Xu, Multi-omics reveals that Bifidobacterium breve M-16V may alleviate the immune dysregulation caused by nanopolystyrene, Environ. Int. 163 (2022) 107191.
[55] L. Zhang, J. Jing, L. Han, Z. Liu, J. Wang, W. Zhang, A. Gao, Melatonin and probiotics ameliorate nanoplastics-induced hematopoietic injury by modulating the gut microbiota-metabolism, Nano Res. 16 (2) (2022) 2885–2894.
[56] Y. Zhang, X. Gao, S. Gao, Y. Liu, W. Wang, Y. Feng, L. Pei, Z. Sun, L. Liu, C. Wang, Effect of gut flora mediated-bile acid metabolism on intestinal immune microenvironment, Immunology 170 (3) (2023) 301–318.
[57] C. Leung, L. Rivera, J.B. Furness, P.W. Angus, The role of the gut microbiota in NAFLD, Nat. Rev. Gastroenterol. Hepatol. 13 (7) (2016) 412–425.
[58] Y. Zheng, J. Wang, J. Wang, R. Jiang, T. Zhao, Gut microbiota combined with metabolomics reveal the mechanism of curcumol on liver fibrosis in mice, Biomed. Pharmacother. 152 (2022) 113204.
[59] J.H. Chen, C.L. Zhao, Y.S. Li, Y.B. Yang, J.G. Luo, C. Zhang, L. Wang, Moutai Distiller's grains Polyphenol extracts and rutin alleviate DSS-induced colitis in mice: modulation of gut microbiota and intestinal barrier function (R2), Heliyon 9 (11) (2023) e22186.
[60] K. Niu, P. Bai, B. Yang, X. Feng, F. Qiu, Asiatic acid alleviates metabolism disorders in ob/ob mice: mechanistic insights, Food Funct. 13 (13) (2022) 6934–6946.
[61] P.D. Cani, C. Depommier, M. Derrien, A. Everard, W.M. de Vos, Akkermansia muciniphila: paradigm for next-generation beneficial microorganisms, Nat. Rev. Gastroenterol. Hepatol. 19 (10) (2022) 625–637.
[62] Y. Yang, M. Li, Q. Wang, H. Huang, Y. Zhao, F. Du, Y. Chen, J. Shen, H. Luo, Q. Zhao, J. Zeng, W. Li, M. Chen, X. Li, F. Wang, Y. Sun, L. Gu, Z. Xiao, X. Wu, Pueraria lobata starch regulates gut microbiota and alleviates high-fat high-cholesterol diet induced non-alcoholic fatty liver disease in mice, Food Res. Int. 157 (2022) 111401.
[63] Y. Saito, T. Sato, K. Nomoto, H. Tsuji, Identification of phenol- and p-cresol-producing intestinal bacteria by using media supplemented with tyrosine and its metabolites, FEMS Microbiol. Ecol. 94 (9) (2018) fiy125.
[64] Z. Yu, D. Li, H. Sun, Herba Origani alleviated DSS-induced ulcerative colitis in mice through remolding gut microbiota to regulate bile acid and short-chain fatty acid metabolisms, Biomed. Pharmacother. 161 (2023) 114409.